

Role of the vortex solid topology in a first-order liquid-solid phase transition

M. Menghini¹, Yanina Fasano^{2,*}, F. de la Cruz², S.S. Banerjee³, Y. Myasoedov³,
E. Zeldov³, C. J. van der Beek⁴, M. Konczykowski⁴ and T. Tamegai⁵

¹*Division of Physics and Astronomy, Faculty of Sciences,
Vrije Universiteit, De Boelelaan 1081,
1081HV Amsterdam, The Netherlands*

²*Instituto Balseiro and Centro Atómico Bariloche, CNEA, Bariloche, 8400, Argentina*

³*Department of Condensed Matter Physics,
Weizmann Institute of Science, Rehovot 76100, Israel*

⁴*Laboratoire des Solides Irradiés, CNRS UMR7642 and CEA-CSM-DRECAM,
Ecole Polytechnique, F-91128 Palaiseau Cedex, France and*

⁵*Department of Applied Physics, The University of Tokyo,
Hongo, Bunkyo-ku, Tokyo 113-8656,*

and CREST Japan Science and Technology Corporation (JST), Japan

Abstract

Using a combination of magnetic decoration and differential magneto-optical techniques we have studied the interrelation between the order of the vortex liquid-solid phase transition and the corresponding structure of the vortex solid phase in $\text{Bi}_2\text{Sr}_2\text{CaCu}_2\text{O}_8$ crystals with different doses of columnar defects (CDs). The magnetic decoration makes evident that when the number of vortices exceeds that of CDs, the vortex solid state is a heterogeneous system containing two species of vortices: A network of grain boundaries associated with vortices pinned on CDs surrounding regions free of columnar defects where Abrikosov microcrystals solidify. On the other hand, when the number of vortices is smaller than that of columnar defects the structure of the vortex solid is amorphous. The vortex liquid-solid phase transition as determined by differential magneto-optical experiments shows that the first-order melting phase transition does not require a structural symmetry break as usually found in nature. Comparative analysis of the topology of the vortex solid and the characteristic of the corresponding melting line reveals a new correlation between the melting mechanisms and the percolation of superconductivity in the heterogeneous vortex solid.

INTRODUCTION

The thermodynamic and transport properties of the mixed state in high and low critical temperature, T_c , superconductors have made evident the different phase diagram of the corresponding vortex structures as a function of field, H , and temperature, T . In low T_c materials the normal-superconducting phase transition in the $H - T$ phase diagram is continuous and well described by the Ginzburg-Landau theory. The associated breaking symmetry is illustrated by a superconducting order parameter that is zero at the transition line, $H_{c2}(T)$. Vortices are generated by superconducting currents that become finite for $H < H_{c2}(T)$. Thus, the topology of the vortex structure is not the consequence of a structural phase transition but rather, it is determined by the competition between vortex-vortex interaction and that between vortices and the pinning potential induced by defects in the atomic structure of the material.

In high T_c superconductors there is a temperature region in the $H - T$ phase diagram where thermal energy prevails over vortex-vortex and vortex-pinning interaction energies. As a consequence, a disordered vortex liquid characterizes the topology of the vortex structure. When cooling, the three energies become comparable and the vortex liquid solidifies at a well defined $T_m(H)$. In clean samples the vortex liquid-solid transformation is achieved through a first-order thermodynamic transition (FOT) at $T_m(H)$ [1–4].

The $H - T$ phase diagram of the vortex system changes drastically in the presence of correlated defects introduced in the atomic structure of the material. In particular, it has been predicted theoretically[5] and shown experimentally [6–10] that the interaction of the vortex system with a strong and correlated pinning potential changes the liquid-solid transition from first to second order. Thus, the vortex system in high T_c superconductors has shown to be a convenient system to study phase transitions of interacting elastic objects in presence of different types of quenched and thermal disorder.

Magnetic decoration experiments performed in clean samples of highly anisotropic high T_c superconductor $\text{Bi}_2\text{Sr}_2\text{CaCu}_2\text{O}_8$ (BSCCO (2212)) have shown that the vortex solid structure in real space is highly ordered [11] in agreement with neutron scattering results showing the Bragg peaks at higher fields [12]. This indicates that even at low fields the vortex mobility at the liquid-solid thermodynamic transition is sufficiently large [13] to avoid the formation of grain boundaries associated with nucleation and propagation of structures grown under

the influence of viscosity, as observed in low T_c superconductors [13, 14].

The highly ordered structure of the vortex solid state as observed [11] in clean BSCCO (2212) samples strongly suggests that this structure could be considered as a good approach to that of the ideal superconducting ground state. This observation has triggered a large effort to develop a theoretical picture that, extending the model proposed years ago by Larkin and Ovchinnikov [15], describes the response of periodic elastic lattices to the presence of quenched and thermally induced disorder preserving the observed quasi-long range order. This was successfully achieved by the Bragg Glass [16] theory. Within this model, the vortex solid presents orientational and translational quasi-long range correlations. Thus, the experimentally observed ordered vortex structure resultant of the liquid-solid first-order phase transition in clean samples is often considered [16–18] as an approach to the ideal Bragg Glass. Furthermore, the detection of solidification through a first-order phase transition together with the observation of a highly ordered vortex structure in the solid state supported the association of this type of phase transition with a change of structural symmetry in analogy with other types of liquid-solid phase transitions found in nature.

The previous statement received a strong support from experiments studying the vortex liquid-solid transition in samples with columnar defects of amorphous material with diameter of the order of 100 Å. These columnar defects generated by heavy ion irradiation induce a correlated potential that interacts with the vortex lattice. It has been observed that the effectiveness of the pinning potential is optimized when the applied magnetic field is nearly parallel to the direction of the columnar defects [6, 7]. The density of these defects is measured in units of magnetic field as $B_\Phi = n_{col}\Phi_0$ where n_{col} is the density of defects and Φ_0 the flux quantum. It has been shown that the randomly distributed columnar defects strongly interacting with vortices transform the first order liquid-solid vortex transition into a second order one [5, 10] where critical exponents and scaling laws determine the electrical transport properties [8] at the liquid-solid transition. The change of symmetry in the second order transition is associated, in this case, with the transformation from an incoherent liquid phase to a coherent superconducting state, as predicted by the Bose Glass theory [5]. This provided further support to the picture sustaining that the first-order liquid-solid transition is associated with a structural symmetry change.

However, the discussed scenario showed inconsistencies when considering the results from local magnetization measurements [9] in samples irradiated with low doses of columnar

defects, $B_\Phi \leq 40$ G. Despite the fact that no differences were found between the melting lines of the pristine sample and the irradiated ones the range of temperatures where the liquid-solid first-order transition took place was limited to higher temperatures and lower fields than those corresponding to the pristine material. The characteristic jump detected in the magnetization was found to disappear at a B_Φ dependent temperature $T_{CP}(H)$: A critical point, CP, in the first-order transition line. The results were interpreted assuming that the pinning potential induced by the low density of columnar defects became ineffective for $T > T_{CP}(H)$, where the quasi-long range topological order would be recovered [9]. This assumption received further support from the experimental results showing that the first-order phase transition takes place even in the range of fields $B < B_\Phi$. If the columnar pinning potential were to remain effective at high temperatures a second order phase transition would be expected [5].

The previous results motivated us to make experiments where the combination of different techniques were used in order to observe the topology of the vortex solid in the field range $B \leq B_\Phi$ and $B > B_\Phi$ [19, 20]. To achieve a better experimental resolution the heavy ion irradiation was made through a mask, allowing the comparison of the thermodynamic transitions in the pristine and irradiated regions as well as the study of the corresponding vortex solid structures in the same sample [19, 20]. These experiments uncovered the interesting result showing that the melting temperature is increased with respect to that of the pristine sample, even for the lowest columnar defect density investigated ($B_\Phi = 5$ G). Besides, the upper end point of the first-order phase transition, T_{CP} , was also observed. Contrary to what was expected, the results made evident that the presence of the low density of columnar defects modifies the melting line in the whole temperature range, even at high temperatures, where melting remains a first-order thermodynamic transition. In Fig. 1 we have plotted the reported [19] melting lines determined by Differential Magneto-Optical (DMO) experiments for the samples studied in this work. For $B_\Phi = 5, 10$ and 50 G a first order phase transition was detected at low fields and high temperatures. As the density of CDs increases a progressive increase of the melting temperature with respect to that of the pristine sample is observed. On the other hand, T_{CP} is shifted to lower fields as B_Φ increases. In the sample with $B_\Phi = 100$ G a continuous liquid-solid phase transition is found in the whole range of fields investigated with DMO, $B < 200$ G. Another striking effect was observed in irradiated samples [19, 21]: a kink in the melting line at $T_{kink} \approx 75$ K that is

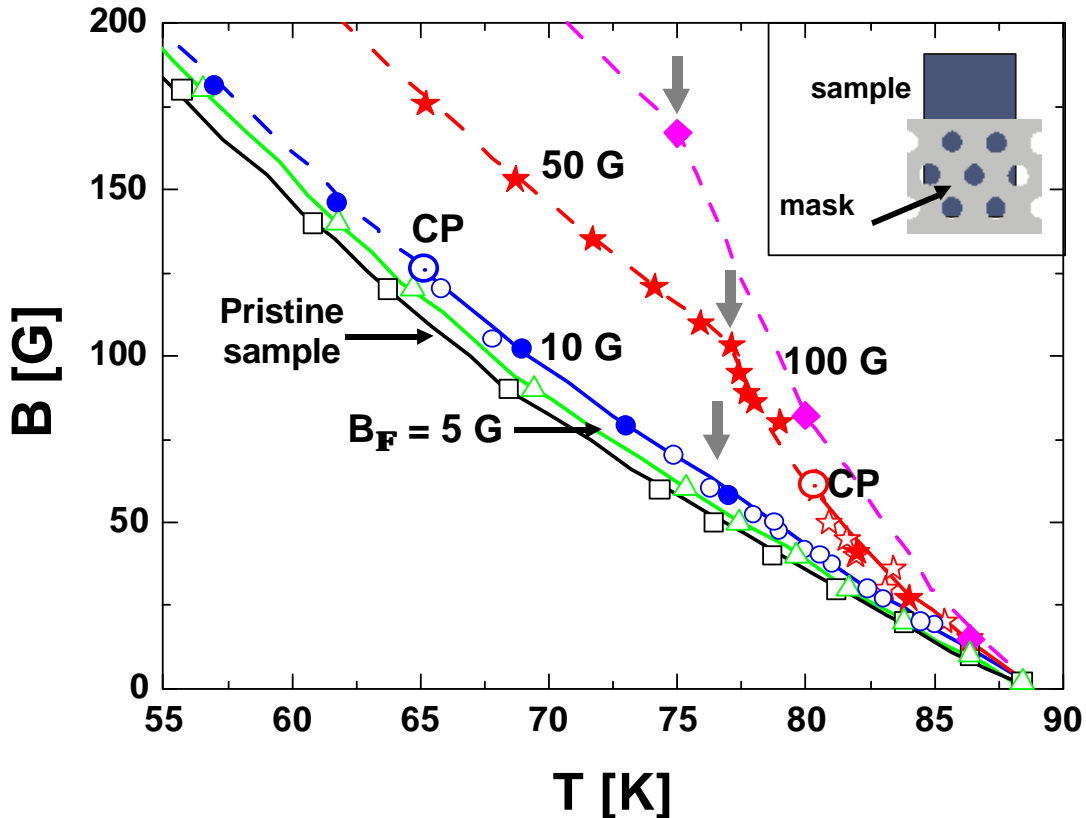


FIG. 1: $B - T$ phase diagram of the vortex system in BSCCO-2212 samples. Vortex liquid-solid phase transition lines in pristine regions and regions with CDs densities corresponding to $B_\Phi = 5, 10, 50$ and 100 G. The open symbols correspond to phase transitions as determined by DMO experiments modulating T (first-order phase transition) while the solid symbols correspond to H modulation. Solid (dotted) lines are guides to the eye of the first-order (continuous) phase transitions. The upper critical end point of the first-order phase transitions are indicated as CP. The vertical thick grey arrows point out the location of the kink in the melting lines. Inset: schematic drawing of the sample and the mask used during the Pb ion irradiation.

almost B_Φ independent, see Fig. 1.

In this work we make an extended comparative analysis of the possible correlation between the vortex structure and the nature of the liquid-solid phase transitions in pristine and irradiated BSCCO(2212) single crystals. The recently discovered intrinsic porous character of the vortex structure in irradiated samples makes evident the heterogeneous nature of vortex matter in this system [19, 20]. When the number of vortices exceeds that of columnar defects, the vortices strongly pinned on columnar defects create a percolating

vortex network throughout the sample. This network is visualized by magnetic decoration as grain boundaries surrounding porous regions, free of columnar defects, where Abrikosov microcrystallites are nucleated. At low fields ($B < B_\Phi$) all vortices are pinned on columnar defects forming a topologically disordered structure. We show that there is no correlation between the polycrystalline or disordered vortex structure and the nature of the liquid-solid transition. However, the characteristic kink found in the melting line [19] is shown to be associated with the field and temperature where the liquid-solid transition changes from the melting of the low field percolating superconducting phase including the rigid skeleton of vortices pinned on CDs) to a region where the melted microcrystals in the pores percolate through the network of the still solid vortex structure pinned in CDs.

EXPERIMENT

We have made a study of the relation between the vortex structure and the nature of the vortex liquid-solid transition in BSCCO(2212) single crystals irradiated with different densities of 1 GeV Pb ions at GANIL (Caen-France). The columnar defects generated by this irradiation were oriented parallel to the crystallographic \hat{c} axis of the sample. The irradiation was made through a stainless steel mask with holes of 90 μm diameter located on top of the sample as depicted in the inset of Fig. 1. In this way, some regions of the sample were left free of columnar defects and the difference between the liquid-solid transitions in pristine and irradiated samples as well as their corresponding structures were resolved with high precision. The liquid-solid phase transition line of these samples was determined using both temperature and field modulation Differential Magneto Optical experiments as described in Ref. 23.

Magnetic decoration experiments were performed to study the topology of the vortex solid phase. This technique consists of evaporating magnetic particles (Fe particles in our case) on the surface of a superconducting sample at low temperatures (4.1 K). The Fe particles accumulated in the regions of maximum magnetic field make a replica of the vortex spatial distribution. The Fe particles remain attached to the surface of the sample even after warming it to room temperature, allowing the analysis of the magnetic decoration experiment by means of SEM. In this article we present results of field cooling, FC, decorations in pristine and irradiated regions of BSCCO(2212) samples with CDs densities of 5, 10, 50

and 100 G. In all cases, the magnetic field, H_a is applied parallel to the CDs direction (\hat{c} crystallographic direction).

MAGNETIC DECORATION RESULTS IN PRISTINE AND HIGH-DOSE IRRADIATED SAMPLES

In Fig. 2(a) a picture of the vortex structure at 40 G in a BSCCO(2212) sample with $B_\Phi = 100$ G obtained by FC magnetic decoration is shown. The picture corresponds to a region where the boundary between irradiated and non-irradiated (left handed) regions can be observed. The DMO experiments in the non-irradiated region of the sample show that the vortex liquid-solid phase transition is characterized by a discontinuity in the vortex density, indicating that the thermodynamic transition is first-order. As expected [11, 16], a hexagonal vortex structure is detected in this region. This is clearly observed by the six peaks of the Fourier Transform of the vortex positions, see Fig. 2(b). On the other hand, the vortex structure in the region with CDs is seen to be highly disordered. In this case, a ring-like Fourier Transform is obtained making evident the loss of orientational order of the vortex structure. Temperature modulation DMO experiments in the irradiated regions of the sample demonstrate [20] that the first-order liquid-solid phase transition has been suppressed. The location of the phase transition line is obtained [19, 20] by field modulation experiments, detecting a continuous transition from the liquid to the solid state. Besides, an increase in the melting temperature with respect to that of pristine regions of the sample is detected in the whole range of fields investigated, see Fig. 1. The observation of a disordered vortex structure is consistent with the expectations from the Bose Glass theory as described in the Introduction.

Note that the vortex structure observed by magnetic decoration does not reflect the equilibrium configuration at the decoration temperature. In the pristine region of the FC sample the vortex liquid solidifies through a first-order phase transition. At the melting temperature, $T_m(H)$, vortex-vortex and vortex-point-defect interactions compete with thermally induced disorder, leading to the quasi-ordered Bragg Glass. As temperature is decreased the pinning potential energy becomes the dominant one, the critical current sets in and the overall vortex structure nucleated at the transition becomes frozen [13]. Thus, the magnetic decoration in the pristine samples shows the ordered (Bragg Glass) vortex structure

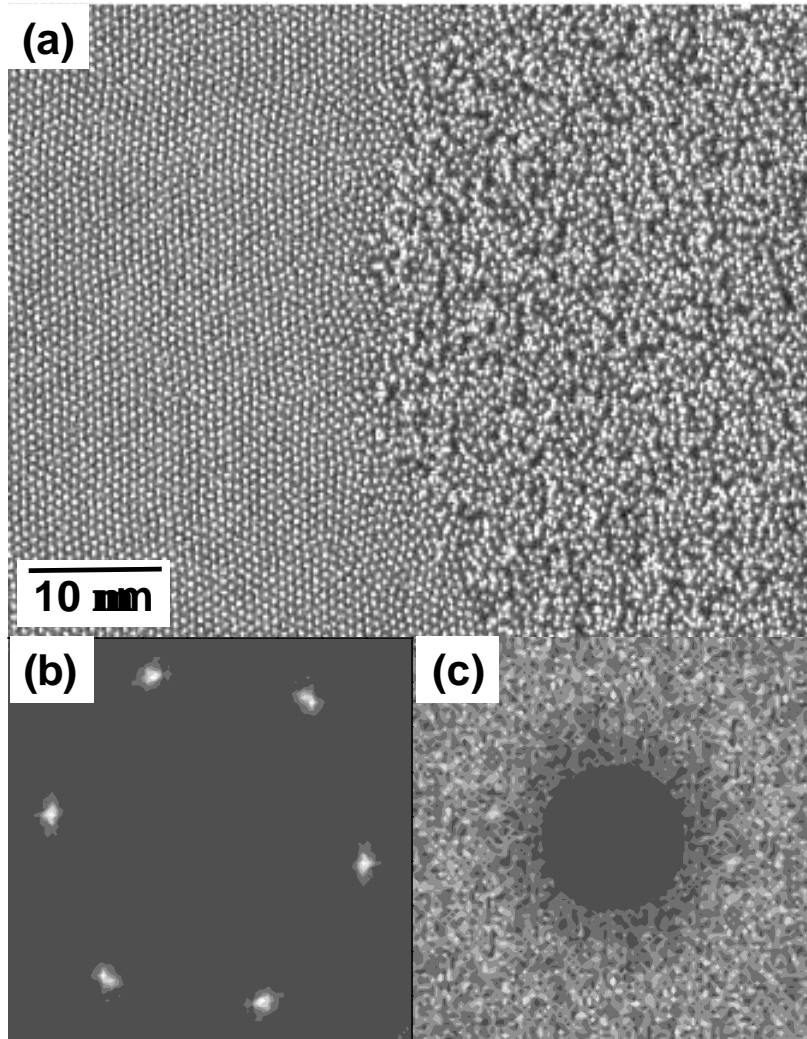


FIG. 2: (a) Magnetic decoration at 40 G in the sample with $B_{\Phi} = 100$ G. The picture shows the boundary between the irradiated and non irradiated regions (right and left side of the image respectively). Fourier Transform of the vortex positions (b) in the non-irradiated and (c) irradiated region.

at a temperature close to $T_m(H)$, where the irreversible behavior is detected. On the other hand, the liquid-solid transition in the irradiated regions with $B_{\Phi} = 100$ G is continuous. The anisotropic pinning potential induced by the columnar defects is stronger than that generated by point defects in the clean sample and the Bose Glass transition for fields applied parallel to the direction of the columnar defects takes place at a temperature higher

than $T_m(H)$ [19]. As in clean samples the topology of the vortex structure, as observed by magnetic decoration, is that of the solid frozen at a temperature close to that of the Bose Glass transition.

VORTEX STRUCTURE FOR LOW IRRADIATION DOSES, $B_\Phi < 100$ G

As it will become clear in what follows, it is convenient to analyze the vortex structure in two different limits $B > B_\Phi$ and $B \leq B_\Phi$.

Vortex structure in the regime $B > B_\Phi$

In this limit the vortex density is higher than that of columnar defects. Magnetic decorations of samples irradiated with $B_\Phi = 5$ and 10 G show that polycrystalline vortex structures are formed for $B = 15, 30,$ and 60 G in the first case and for 40 and 80 G in the second one. As example, Delaunay triangulations of the vortex structure are shown in Fig. 3. The triangulation consists of joining with straight lines each vortex with its nearest neighbors. In the figure the black dots indicate topological defects of the structure, that is, vortices with coordination 5 or 7. As it is clearly observed from the figure most of the topological defects are arranged forming grain boundaries.

It is important to remark the difference between these grain boundaries and those associated with the vortex polycrystalline structure [11, 13] when FC the low T_c superconductor NbSe₂ with no CDs. In that case the formation of a polycrystal is associated [13] with a nucleation and growth process of the vortex structure in the presence of uncorrelated pinning potential generated by the defects naturally present in the samples. In low T_c superconductors the vortex structure nucleates at $T_{c2}(H)$ and the detection of a finite critical current just below this transition line indicates that the interaction of the vortices with the pinning potential competes with the vortex-vortex interaction when the vortex structure is formed. Thus, in NbSe₂ crystals the increase of the vortex-pinning interaction when cooling precludes the formation of a vortex single crystal.

In the case of NbSe₂ it is possible to generate a vortex single crystal using the Field Cooling Rotation (FCR) process [24]. This procedure consists of moving the vortices at high velocities and performing the decoration after removing the driving force. Experimentally

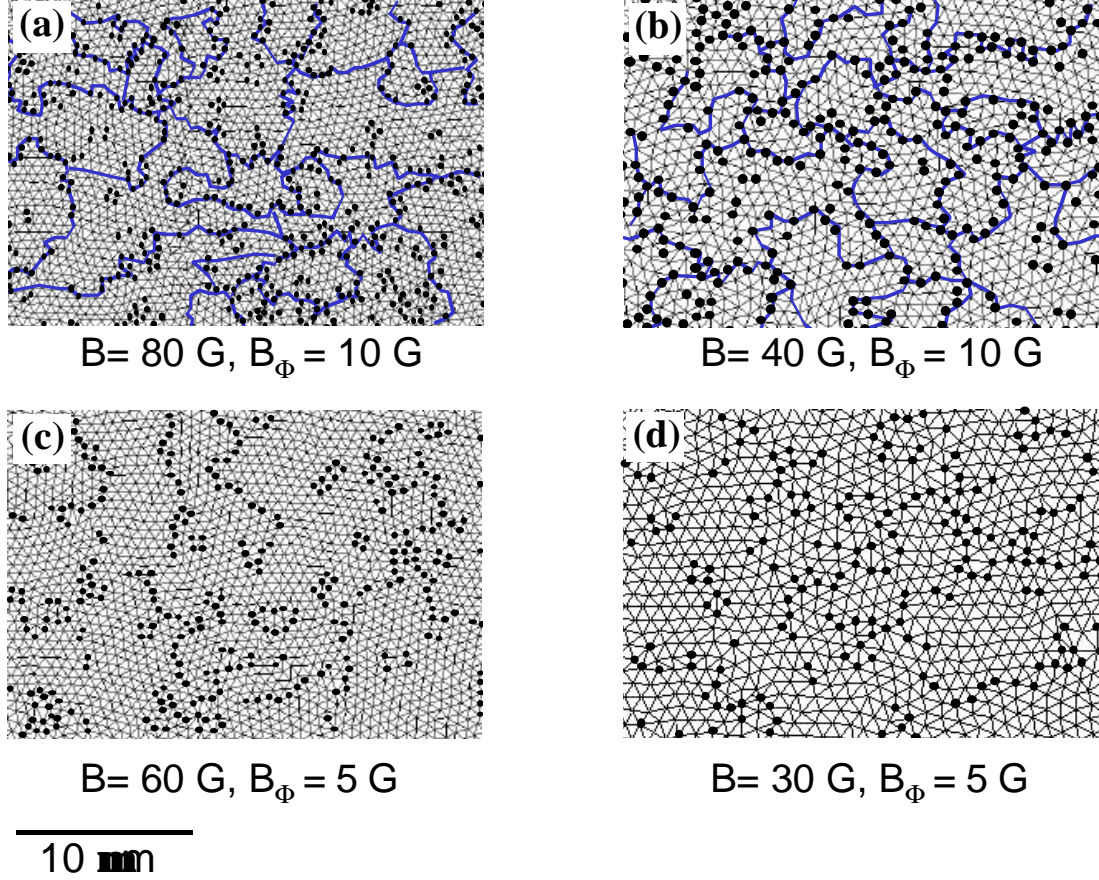


FIG. 3: Delaunay triangulations of the vortex structures obtained at (a) 80 and (b) 40 G in the sample with $B_{\Phi} = 10$ G and (c) 60 and (d) 30 G in the sample with $B_{\Phi} = 5$ G. The black dots indicate topological defects of the vortex structure. As an example in (a) and (b) we indicate with thicker lines the grain boundaries of the vortex structure as defined in the text.

this is achieved by cooling in the presence of a field perpendicular to the surface of the sample (\hat{c} direction) down to the rotation temperature, T_{rot} , then a transverse magnetic field, H_T , is applied and removed suddenly. This rapid variation of the in-plane magnetic field induces currents in the sample that generate the movement of the vortices. Finally, the decoration is made at $T_{dec} \leq T_{rot}$. The previous results in NbSe_2 samples promoted us to use the same method in $\text{BSCCO}(2212)$ samples with CDs in order to verify whether it is possible to generate vortex single crystals.

In Fig. 4(a) an image of the FCR magnetic decoration in irradiated $\text{BSCCO}(2212)$ samples with $B_{\Phi} = 10$ G is shown. In this experiment the field in the \hat{c} direction was 40 G and the field in the transverse direction, applied and removed at 4.1 K, was 80 G. The direction of

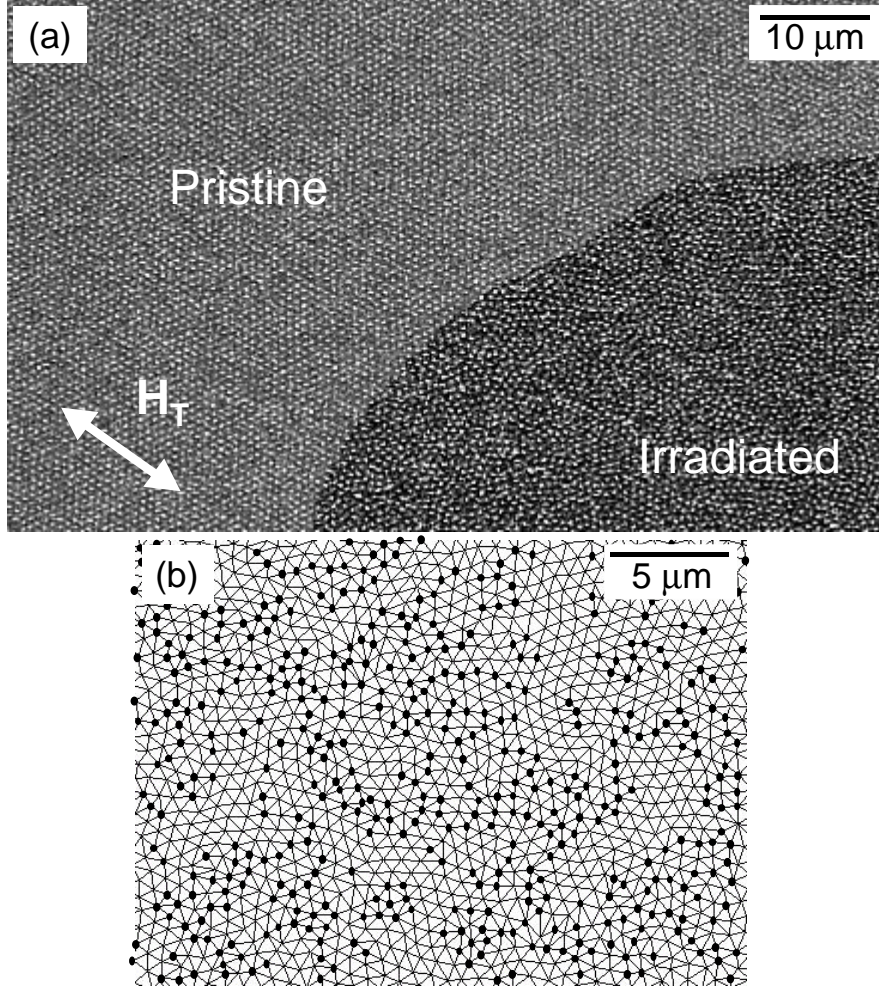


FIG. 4: (a) FCR magnetic decoration with $H_a = 40$ G and $H_T = 80$ G in the $B_\Phi = 10$ G sample. The direction of H_T is indicated by the arrow. The darker area of the image corresponds to the irradiated region. (b) Delaunay triangulation of the FCR vortex structure in the irradiated region.

the in-plane field is indicated by the white arrow. As was previously observed the vortex structure in the pristine region is oriented in the direction of the transverse field [13]. A Delaunay triangulation of the vortex structure in the irradiated region is shown in Fig. 4(b) making evident that the structure is polycrystalline. In this case, no alignment of the crystalline regions with respect to the in-plane field is observed. It can be argued that the transverse field applied at low temperatures does not penetrate the irradiated regions due to the strong pinning induced by the columnar defects. If this were the case the vortices in the neighborhood of the irradiated region should show an orientation determined by the shielding currents. A uniform and ordered distribution of vortices was observed in the

surroundings of the irradiated circles disregarding the previous suggestion.

The results of FCR experiments support that the polycrystalline vortex structure in irradiated BSCCO(2212) samples is stabilized by the space distribution of CDs. In order to determine the relation between the topology of the polycrystal and the distribution of CDs in the sample we have made a detailed analysis of the observed vortex polycrystalline structure.

We have counted the number of vortices in each grain, N_{vg} , in order to determine the grain size for each B and B_Φ . The grain boundaries that separate different grains are defined as the contours between vortex crystallites that differ in orientation in 10° or more. We have analyzed areas of the samples containing of the order of 5000 vortices. We found that for each applied field there is a broad distribution of N_{vg} where a maximum and a minimum value can be defined. This result is consistent with a uniform distribution of grain sizes for each B and B_Φ . In Figure 5 we plot the maximum and the minimum value of N_{vg} as a function of B . Fig. 5(a) corresponds to $B_\Phi = 10$ G and (b) to $B_\Phi = 5$ G. As it is clearly seen from the figure, N_{vg} grows linearly with B for each B_Φ . Taking into account that the number of vortices within a given area A is $N_A = BA/\Phi_0$ the results show that the area of the largest and the smallest grain for a given B_Φ are independent of B .

Defining the average number of vortices in grains, $\langle N_{vg} \rangle$, as the ratio between the

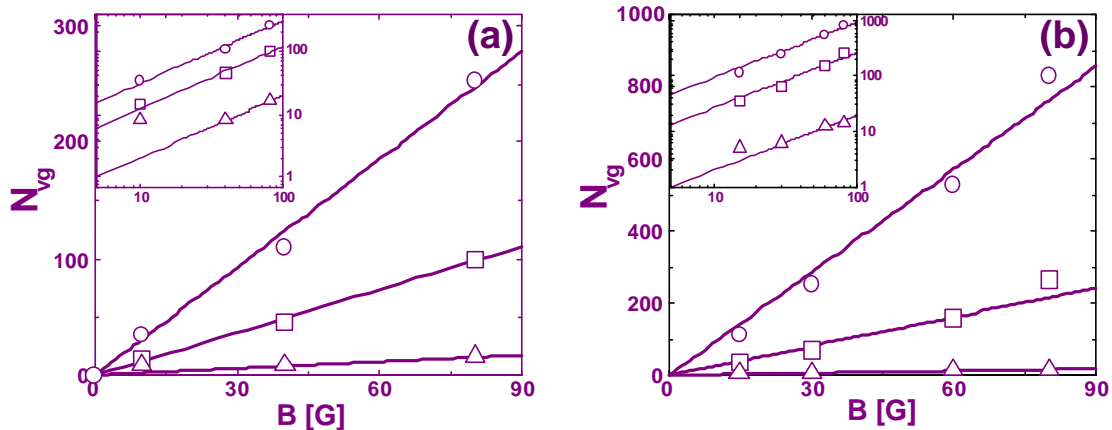


FIG. 5: Number of vortices within grains N_{vg} as a function of B for (a) $B_\Phi = 10$ G and (b) $B_\Phi = 5$ G. The circles (triangles) correspond to the number of vortices within the largest (smallest) grains. The average number of vortices within grains are indicated with squares, see text. Inserts: log-log scale of the plots shown in the corresponding main panels.

total number of vortices within grains and the number of grains, we found that $\langle N_{vg} \rangle$ also grows linearly with B , showing that the distribution of N_{vg} is the same in the field range investigated. The B independence of the grain areas of the polycrystalline structure in the irradiated regions strongly supports that both, the spatial distribution as well as the size of the grains are determined by the CDs landscape.

It is then relevant to find out what is the spatial distribution of CDs. This was achieved etching a mica sample, irradiated simultaneously with the BSCCO(2212) crystals. Figure 6(a) shows a typical distribution of CDs as detected by an AFM imaging. In this case, the irradiation corresponds to $B_{\Phi} = 5$ G. In Fig. 6(b) we show a distribution of random points generated numerically with a density corresponding to $B_{\Phi} = 10$ G, showing an indistinguishable space distribution when compared with that of Fig. 6(a) with the appropriate rescaling of lengths corresponding to the different densities. The relevant characteristic of the random distribution of points for our analysis is its apparent inhomogeneous distribution at the scale of the average distance between vortices.

The described polycrystalline vortex structure and the observed inhomogeneous distribution of CDs surrounding voids with different areas, as depicted in Fig. 6(a), suggest that the FC solidification process of the vortex structure takes place in two steps. First the vortices nucleate on the CDs, developing a percolating vortex network of strongly pinned vortices surrounding regions free of CDs. The rigid vortices of the network determine the space orientation of the subsequently solidified microcrystallites nucleated within the regions free of CDs. The network of pinned vortices precludes the propagation of the orientation of the ordered vortex structure beyond the limits imposed by their distribution in space, giving rise to the observed grain boundaries. To clarify this, we show a small portion of a vortex lattice at a field of 30 and 40 G together with the distribution of random points, insets of Fig. 6(a) and (b) respectively. It is evident that the inhomogeneous spatial distribution of random CDs is compatible with the formation of microcrystallites randomly oriented, surrounded by localized vortices residing on almost all CDs. The rigid network of interacting vortices localized on CDs is represented in Fig. 6(b) by the circles centered in the location of the random points with a radius of the order of the interaction range between vortices, the penetration depth, λ . In this particular case we have considered the vortex structure corresponding to 40 G. Since the vortex configuration is frozen at a temperature close to the melting temperature the appropriate interaction distance is $\lambda(T_m) \approx 0.4 \mu\text{m}$ as calculated

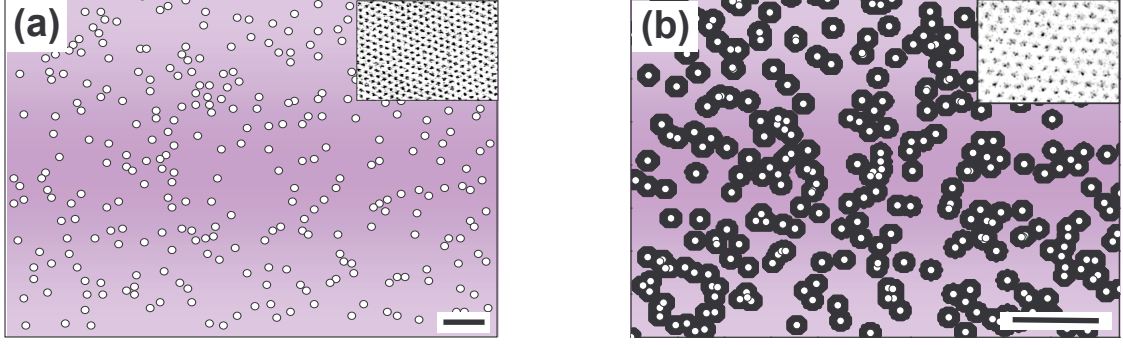


FIG. 6: (a) Distribution of CDs in a mica sample irradiated with $B_\Phi = 5$ G. (b) Random distribution of points (white points) generated numerically with $B_\Phi = 10$ G. The black circles indicate the interaction range between vortices at $T_m(40$ G) (see text). The scale bars correspond to $5 \mu\text{m}$. Insets (a) and (b): Vortex lattices in the pristine regions at 30 and 40 G, respectively.

using T_m obtained by DMO experiments in the sample with $B_\Phi = 10$ G. It is clear that the vortices localized on CDs form a barrier for the propagation of a vortex single crystal throughout the sample in the range of fields discussed in this work.

The results discussed previously show that the vortex matter in the presence of CDs is heterogeneous, consisting of two species of vortices: One associated with the grain boundaries induced by the rigid skeleton of vortices localized on the CDs, ρ_{cont} , and the other forming the small Abrikosov crystallites surrounded by the grain boundaries, ρ_{crys} . It is important to note that the relative density of the CDs and vortices and the condition that each CD localizes no more than one vortex, impose a geometrical constraint for the formation of a polycrystalline structure.

Vortex structure in the regime $B \leq B_\Phi$

Considering the previously mentioned distinction between two types of vortices it is expected that when the ratio between vortices and CDs decreases a disordered vortex structure will be formed, consistently with the condition $\rho_{crys} \rightarrow 0$. In particular, one could imagine that when the density of vortices equals that of CDs the structure obtained by magnetic decoration would resemble the distribution of CDs. Contrary to this expectation, the vortex structure is not as disordered as the distribution of CDs in this case, see Fig. 7(a). The differences between the vortex structure for $B = B_\Phi$ and the corresponding distribution of

CDs are made evident when comparing the pair distribution distribution functions, $g(r)$, that is the probability to find two particles separated by a distance r . In the case of the vortex structure shown in Fig. 7(a) $g(r)$ presents two peaks indicating short range positional correlation (see Fig. 7(b)). Besides, $g(r)$ is null for $r < r_0$, making evident that as a consequence of the repulsive interaction between vortices there is no double occupancy of vortices on the columnar defects. This last statement is experimentally verified by comparing the density of vortices in the pristine and the irradiated regions. On the other hand, no short range positional order is detected in the distribution of CDs as expected for tracks generated by ion irradiation (see Fig. 7(c)).

Thus, we see that for $B = B_\Phi$ not all the vortices are on CDs implying that $\rho_{cont} \neq 1$

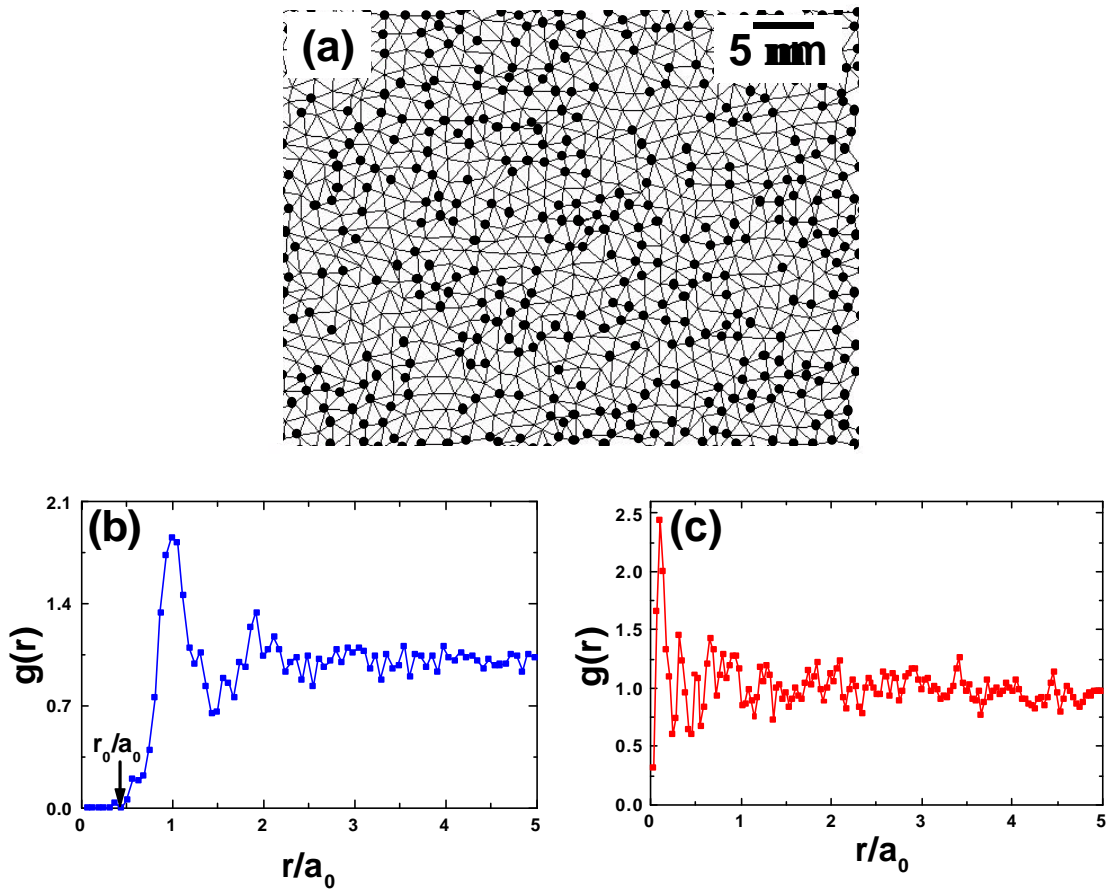


FIG. 7: (a) Delaunay Triangulation of the vortex structure at 4.1 K and 10 G in the $B_\Phi = 10$ G sample. (b) and (c): Pair-distance distribution functions of the vortex structures shown in (a) and of the random distribution of points shown in Fig. 6(b), respectively.

and $\rho_{crys} > 0$. This is reasonable since in the distribution of CDs there are still voids free of CDs where a finite number of vortices can be fitted with a density compatible with the value of B while some of the closely packed CDs may remain unoccupied. We have defined vortex grains as in the case $B > B_\Phi$ for the structure shown in Fig. 7(a) where $B = B_\Phi = 10$ G. We have found that N_{vg} for the largest grains fits very well the B linear dependence (see Fig. 5(a) insert). On the other hand, the value of N_{vg} for the smallest grain is larger than the one expected. This can be understood considering that the area of the smallest grains that were found B independent in the range $B > B_\Phi$ become now field dependent. This is because the rigid skeleton of vortices pinned on CDs surrounding the smallest areas free of CDs encloses areas too small to form both microcrystals as well as the corresponding grain boundaries, as will be discussed in the next section. The detected vortex structure for $B = B_\Phi$ is consistent with the results of numerical simulations in the regime $B \approx B_\Phi$ taking into account the repulsive interaction between vortices [25]. The authors in Ref. 25 found that all the vortices are localized on defects only when they consider $\lambda/d = 0$, where d is the distance between CDs. As soon as λ/d is finite, the value of B/B_Φ where all vortices are localized in CDs is lower than 1 and decreases with λ/d , in agreement with our results.

We have found that for $B = B_\Phi$ a small fraction of vortices prefers to form crystallites in regions free of CDs instead of localizing on them. This is an indicator of the relevance of the competition between vortex-vortex and vortex-CD interaction. For low vortex densities as compared with that of CDs the vortex system gains from CDs pinning potential without a significant increase of elastic energy. In the dilute limit it is always possible to find CDs on which the vortices can pin while preserving the average distance imposed by the field. One example of this is shown in Fig. 8(a) where the FC vortex structure obtained at 40 G in the sample with $B_\Phi = 100$ G is depicted. The corresponding Delaunay triangulation is shown in Fig. 8(b).

The ground state of vortices in the presence of CDs in the regime $B < B_\Phi$ has been extensively studied in Ref. 26 by Monte Carlo simulations. Since the interaction between vortices is taken into account, the relevant parameters in the simulations are the average distance between vortices, a_0 , the distance between CDs, d , and the range of vortex-vortex interaction, the penetration length, λ . The authors found that for $B/B_\Phi < 0.4$, and considering a logarithmic vortex-vortex interaction, all the vortices are localized on CDs and the vortex structure presents a high density of topological defects, ρ_{def} . In that case, it was

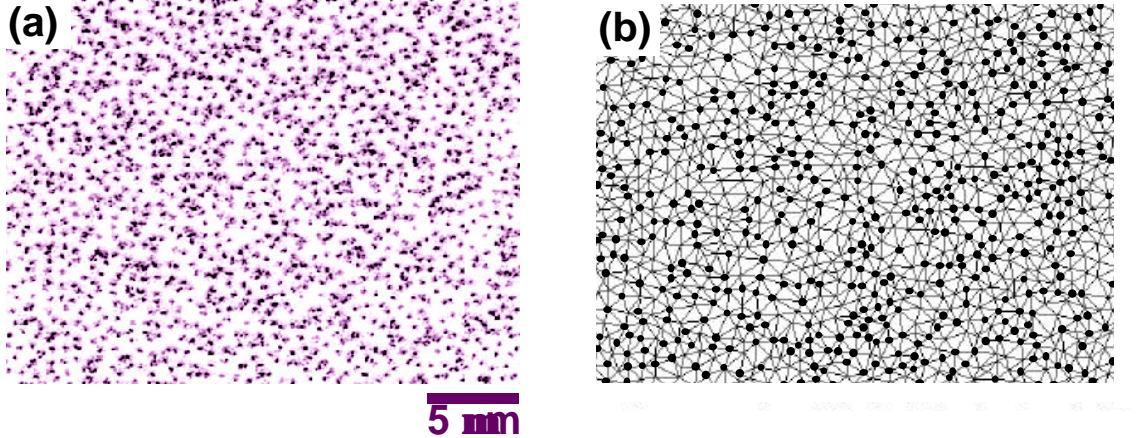


FIG. 8: (a) FC magnetic decoration and (b) corresponding Delaunay triangulation of the vortex structure at 4.1 K and 40 G in the $B_{\Phi} = 100$ G sample.

reported that $\rho_{def} = 0.43$ for $B/B_{\Phi} = 0.4$, in agreement with the decoration experiments where we find $\rho_{def} = 0.43$ for the same value of B/B_{Φ} in the sample with $B_{\Phi} = 100$ G, see Fig. 8. Besides, we find that the distribution of the distance between first nearest neighbors of the two structures, the one obtained by simulations and the experimental one, are qualitatively the same. In both cases the distribution is Gaussian with a standard deviation of $0.25a_0$ [26].

The results presented in this section show that for $B/B_{\Phi} \leq 1$ the experimental distribution of vortices in the sample is the consequence of vortex localization on CDs separated by distances determined by the repulsive interaction between vortices. As a result of the competition between the pinning and vortex-vortex interaction energies a highly disordered vortex structure is formed for $B = B_{\Phi}$ that becomes amorphous for $B < B_{\Phi}$.

MODEL FOR THE FRACTION OF TOPOLOGICAL DEFECTS

The previous results provide strong evidence for the heterogeneous behavior of the vortex matter in the range of B and B_{Φ} investigated in this work. Thus heterogeneity rather than homogeneity should characterize the structural, thermodynamic and transport properties of vortex matter in irradiated materials. The distinction of two species of vortices allows us to propose a model to describe the behavior of the fraction of topological defects as a function of B and B_{Φ} [20]. Since the grain boundaries detected by magnetic decoration are made

evident by topological defects induced by the vortex localization on CDs surrounding small crystallites, we assume that $\rho_{cont} \propto \rho_{def}$, where ρ_{def} is the fraction of topological defects. In an arbitrary area A of the sample and for each value of B the number vortices in grain boundaries is proportional to $N_{cont} = L/a_0$ where L is the total length of the contours enclosed in A and a_0 is the lattice parameter of the corresponding Abrikosov structure associated with B . The analysis of the number of vortices within grains has shown that the area of the grains does not change with B . This means that the perimeter of these areas should also be B independent, and hence L is only function of B_Φ . Therefore,

$$N_{def} \propto L(B_\Phi)/a_0 \propto L(B_\Phi)B^{1/2} \quad (1)$$

where we have considered that $a_0 \propto B^{-1/2}$. In order to determine the dependence of L on B_Φ we have to determine the change in the length of the contours when the density of CDs varies. It is important to notice that the space configurations of different densities of randomly distributed points are self-similar, meaning that the structure is invariant under isotropic scale transformations. If the density of CDs increases by a factor of m then, the size of the areas enclosed by the contours will be reduced by a factor of m . Consequently, the length of individual contours will be reduced by a factor of \sqrt{m} . On the other hand, the total number of contours increases as the density of CDs, m . Finally, the total length of the contours increases by \sqrt{m} when B_Φ increases by a factor of m , and therefore $L(B_\Phi) \propto \sqrt{B_\Phi}$. Considering this in Eq. 1 we obtain that $N_{def} \propto \sqrt{B_\Phi B}$. Thus, our simple model predicts that the fraction of topological defects of the vortex structure would be

$$N_{def}/N_v = \rho_{def} \propto \sqrt{B_\Phi/B} \quad (2)$$

The proportionality constant is determined by the geometry of the contours defined by the CDs, and consequently it is difficult to determine it *a priori*. In Fig.9 we plot the results of ρ_{def} for the samples with $B_\Phi = 5, 10, 50$ and 100 G. The agreement between the experimental data and the prediction of the model (solid line) in the regime $B > 1.7B_\Phi$ ($B_\Phi/B < 0.59$) is evident. The disagreement between the model and the experiment in the regime where the number of vortices is of the order and smaller than the number of columnar defects is easily understood. The main assumption in the derivation of the functionality of ρ_{def} with B and B_Φ is that the number of topological defects is proportional to the number

of vortices in contours. Besides this, we considered that N_{cont} can be measured in units of the vortex lattice parameter as L/a_0 , where L is the total length of the contours. In the previous section we have shown that in the regime $B < B_\Phi$ the spatial distribution of vortices is determined by the energy balance between localizing vortices on CDs and the interaction between vortices. In this limit, where the number of CDs exceeds that of vortices many of the contours that would define a vortex grain has a length of the order of a_0 or even smaller. Thus, even though the vortices are on CDs, a_0 is not an appropriate scale to measure L in this case. This explains the deviation from the model observed for $B < 1.7B_\Phi$. Moreover, we have found that in this regime $\rho_{def} \approx 0.5$ for all the values of B/B_Φ investigated in agreement with numerical simulations [26].

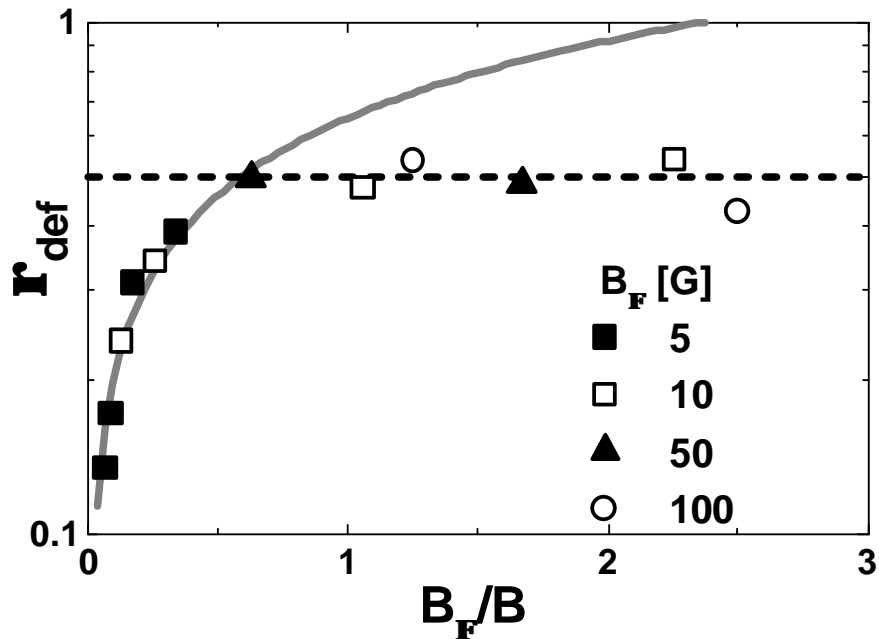


FIG. 9: Density of topological defects of the vortex structure, ρ_{def} , as a function of B_Φ/B for different values of B_Φ .

VORTEX STRUCTURE AND LIQUID-SOLID PHASE TRANSITION

The DMO measurements in the sample with $B_\Phi = 100$ G show that the first-order liquid-solid phase transition has been suppressed by the presence of CDs in the whole range of fields investigated, $B < 200$ G. The evidence of a phase transition in this sample is associated

with the detection of an irreversibility line by means of DMO measurements modulating the magnetic field [20]. Magnetic decoration experiments in the regime $B < B_\Phi$ in this sample show a disordered vortex solid structure, see Fig. 8. As we explained in the previous sections this is consistent with the proposed model of two vortex species and the condition $B < B_\Phi$. In this case we could interpret the results as a consequence of a continuous phase transition between two disordered structures, one liquid and the other an amorphous solid. The possible symmetry breaking could be associated with the onset of superconducting Bose Glass state.

On the other hand, the results for lower doses of columnar defects were found surprising. The DMO experiments in BSCCO-2212 samples with CDs densities of 5 and 10 G show that the liquid-solid phase transition in the irradiated regions remains first-order at low fields, even though the whole melting curve is displaced to higher temperatures as compared with that in pristine regions, see Fig. 1. The high sensitivity of the DMO technique and the comparative studies made in the pristine and irradiated regions of the same sample allow the understanding of the possible inconsistencies mentioned in the Introduction. The melting temperature, $T_m(H)$, of the irradiated samples is seen to shift upwards with respect to that of the pristine sample. This makes evident that CDs create an effective pinning potential in the whole range of temperatures, up to T_c . Despite this the liquid-solid transition is first-order.

By means of FC magnetic decorations we were able to observe the heterogeneous nature of the vortex matter in the presence of CDs. The decoration made evident the existence of a skeleton of vortices localized on CDs that precludes the propagation of the crystalline or Bragg Glass structure throughout the irradiated region. It could be argued that the local order shown by the Abrikosov crystallites is enough to allow the first-order phase transition as observed in most of polycrystalline solids. This argument can be readily discarded because the melting line for low doses of CDs is also shown to be first-order even at $B < B_\Phi$, where no crystallites are present, see Fig. 1.

An interesting behavior of the vortex system for intermediate irradiation densities is also detected. For $B_\Phi = 50$ G a first-order liquid-solid phase transition is measured in the regime $B < B_\Phi$, see Fig. 1. Following the distinction between vortices in networks determined by CDs and vortices in crystallites, we expect that the vortex structure is disordered with $\rho_{def} \approx 0.5$ in this field regime. This is clearly observed in Fig. 10(a) and (b) corresponding to a FC

decoration at 30 G in a sample with $B_{\Phi} = 50$ G. As discussed before, due to the repulsive interaction between vortices the pair correlation function becomes zero below a minimum distance, r_0 , between first near neighbors. The results in Fig.10(c) show that, for this particular case, the value is $0.4a_0$. Considering $\lambda(0) = 0.2 \mu\text{m}$ for BSCCO(2212) and using the minimum distance between vortices provided by the pair correlation function, r_0 , as the penetration depth at the temperature where the structure is formed we obtain a temperature $T = 81.5 \pm 1$ K. The results of DMO experiments indicate that the melting temperature for this structure is 83.1 K, in a very good agreement with our estimate. The good agreement between these two values confirms that the observed topology of the vortex structure is that formed at the liquid-solid phase transition. As a consequence, this experimental data provides an independent support that the observed amorphous structure is only determined by the ratio B/B_{Φ} , independently of the order of the liquid solid phase transition. Thus, the combination of DMO and decoration experiments made in the same samples show that there is no necessary correlation between the topology of the solid phase and the order of the melting transition.

The described heterogeneous characteristics of the vortex system provide a new scenario for the understanding of the structural and superconducting properties of the vortex matter in the presence of columnar defects. Structural, DMO and transport studies [22] in the range $B/B_{\Phi} < 1.7$ show that the liquid-solid transition line (either through first or second order thermodynamic transitions) marks the formation of the disordered vortex structure associated with vortices mainly localized on CDs. In this limit the loss of superconducting phase coherence in the $a-b$ planes at the melting temperature coincides with the fusion of the disordered structure. The situation is less clear in the field range $B/B_{\Phi} > 1.7$. As discussed previously, the vortex matter in the solid phase is heterogeneous composed by a disordered specie associated with vortices pinned on CDs (visualized as grain boundaries) caging small ordered vortex crystallites. In this regime the disordered specie precludes the propagation of crystalline order across the sample. However, in the solid state the superconducting phase coherence is established in both vortex species throughout the sample. The DMO technique detects the melting of the solid state either by thermodynamic measurements when the transition is of first-order or by field modulation when the transition is continuous. As decoration in the liquid cannot be made, the technique cannot provide information on whether there is a homogeneous liquid in the sample at the melting temperature or, as

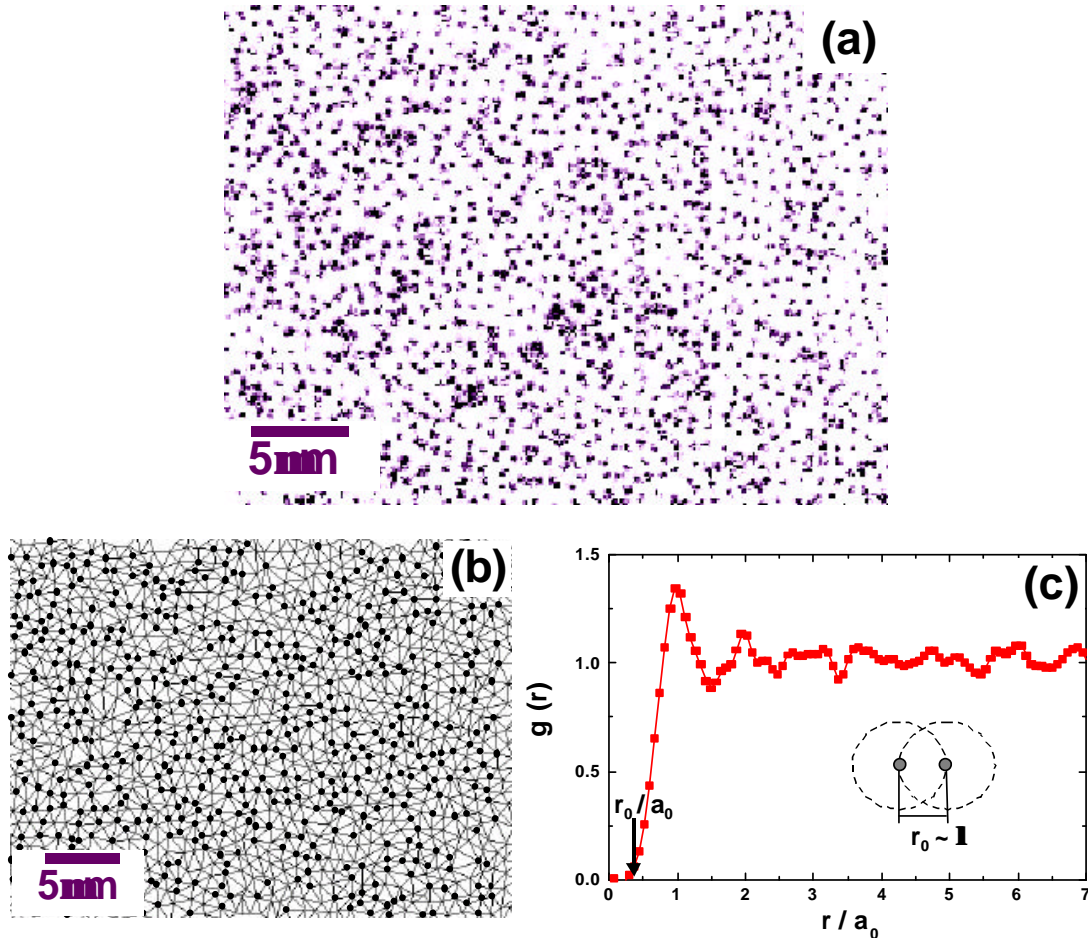


FIG. 10: (a) FC magnetic decoration, (b) Delaunay triangulation, and (c) pair distribution function of the vortex structure at 4.1 K and 30 G in the $B_\Phi = 50$ G sample. In (c) the black vertical arrow marks the distance $r_0 \approx \lambda(T_m)$ where the pair correlation function becomes different from zero, see text.

was previously suggested [19, 27, 28] there is a liquid coexisting with vortices pinned on CDs. Recent transport measurements [22] clearly show that in the $B/B_\Phi > 1.7$ limit the vortices on CDs remain pinned to temperatures well above that of the melting, showing that the solid-liquid transition should be associated with the melting of the small crystallites. However, it is important to remark that the detection of melting by the DMO technique implies the loss of the superconducting phase coherence in the $a - b$ planes. Thus, despite the fact that vortices remain pinned by the CDs, the melting as detected by a change in magnetization implies the interconnection of vortex liquid droplets across the sample. This discussion indicates for the first time a unique interrelation between the melting curve and

the observed heterogeneous vortex structure.

CONCLUSIONS

By means of magnetic decoration we have been able to determine the topology of the vortex solid phase in the presence of CDs. The analysis of these results together with the $H-T$ phase diagram obtained by DMO in the same samples have allowed us to demonstrate the lack of correlation between the topology of the vortex structure and the thermodynamic order of the liquid-solid phase transition.

We have observed that in the presence of CDs the vortex solid matter in the range of fields investigated is a heterogeneous system associated with vortices forming grain boundaries comprising a disordered structure surrounding small Abrikosov crystallites. In the case $B > 1.7B_\Phi$ the correlated defects stabilize a polycrystalline vortex structure where the grain boundaries are fully determined by the distribution of CDs and we modeled the behavior of ρ_{def} with B and B_Φ considering that vortices are divided in two species, a topologically disordered one associated with the grain boundaries induced by the rigid skeleton of vortices on CDs and the other associated with the small ordered Abrikosov crystallites. In the limit $B < 1.7B_\Phi$ the vortex structure is amorphous with a density of topological defects $\rho_{def} \approx 0.5$, in agreement with Ref. 26. In this regime the vortex solid topology is mainly determined by the vortices pinned on CDs at an average distance given by the interaction range between vortices, $\lambda(T_m)$, at the temperature where the solid structure is formed. The magnetic decoration results are summarized in Fig.11. In this figure we have drawn a horizontal line at $B = 1.7B_\Phi$ indicating the crossover from a region where the heterogeneous solid is stabilized at higher fields to a highly disordered structure that becomes fully amorphous at lower fields. As the magnetic field is decreased below this line the largest regions free of CDs may still contain vortex crystallites, while the smallest regions free of CDs can no longer be filled by crystallites. When further decreasing the field all the regions free of CDs, even the largest, become empty. Vortices become pinned on CDs, forming an amorphous structure with a near neighbor short range correlation determined by the interaction energy between vortices.

The analysis of these results in the framework of liquid-solid phase transition leads us to an unexpected conclusion. The topological quasi-long range order, characteristic of the

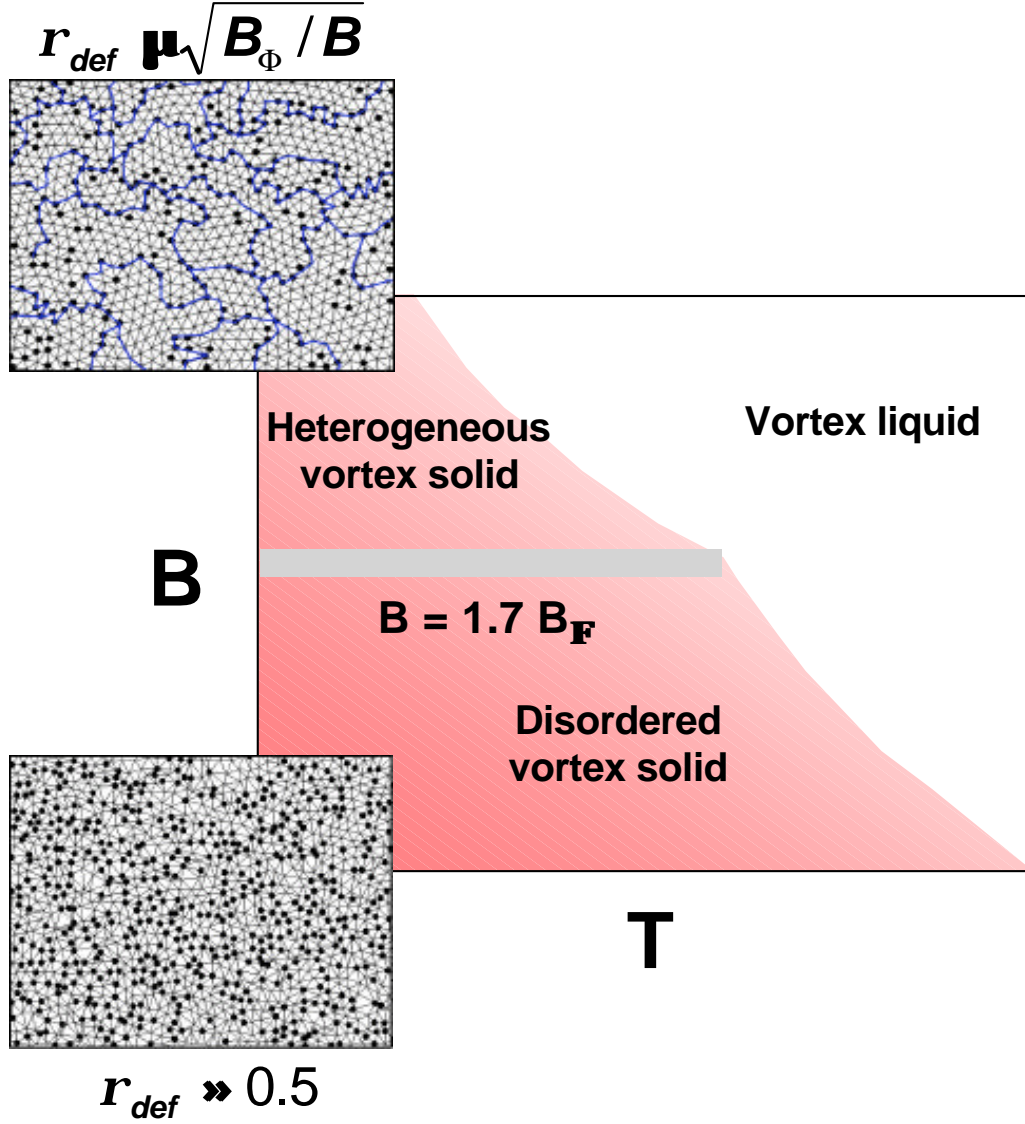


FIG. 11: Schematic $B - T$ phase diagram of the vortex system in the presence of columnar defects with $B_\Phi > 50\text{G}$ where the kink in the melting line coincides with the percolation of liquid nanodroplets, see text. The boundary line that separates the vortex polycrystal from the amorphous phase is shown.

Bragg Glass, is not a necessary condition for the existence of a FOT. Moreover, we have observed that the vortex liquid is transformed into an amorphous solid through a FOT. Thus, the finite step in the equilibrium magnetization at FOT is not associated with the break of a structural symmetry in the $a - b$ plane. By means of Josephson Plasma Resonance experiments it has been suggested that the melting transition in clean BSCCO-2212 samples

is induced by a softening of the Josephson coupling in the \hat{c} direction [29]. Thus, it will be interesting to determine whether this decoupling transition also occurs in samples with low density of CDs. If this is the case, then the FOT line separates a phase decoupled in the \hat{c} direction from one with a finite coupling and with quasi-long range, short-range or no positional order depending on the ratio B/B_Φ .

As discussed above, vortex decorations have identified two field regimes for a given B_Φ . At low fields the vortex solid is only associated with the superconducting skeleton of vortices pinned on CDs; consequently the melting of the skeleton and the loss of phase coherence in the $a - b$ plane coincide at the melting temperature. In the high field limit the detection of melting by DMO implies the loss of phase coherence in the $a - b$ planes. This could be either due to the melting of the superconducting skeleton or to the loss of superconducting percolation induced by the interconnection of liquid droplets melted in the voids of the vortex structure. In the last case this is achieved by the formation of an interconnected liquid [22] percolating between vortices that remain pinned on the CDs. The inspection of melting curves show the presence of a sharp kink suggesting a change of regime in the melting process, as proposed in Ref. [19]. Since the kink in the melting curve is detected independently of the order of the melting transition it is reasonable to link its origin with a change of the mechanism inducing the loss of superconducting coherence.

The combination of the decoration results and the measurement of $B_{kink}(B_\Phi)$ from the melting curves allows us to determine the vortex structure when the change in the melting regime takes place. In Fig. 12 we have added the experimental values of B_{kink}/B_Φ for different B_Φ [19]. The results make evident that for $B_\Phi > 40\text{G}$ the kink coincides with the value of B/B_Φ where crystallites are formed within the voids. In other words $B > B_{kink}$ implies $B > 1.7B_\Phi$, showing that the percolation of the liquid takes place as soon as the Abrikosov crystallites melt as droplets in the voids. On the contrary, the rapid rise of B_k at lower B_Φ indicates that in this region superconductivity percolating along the rigid vortex skeleton is strong enough to avoid either the melting of the crystallites or to sustain the liquid droplets without percolating across the sample.

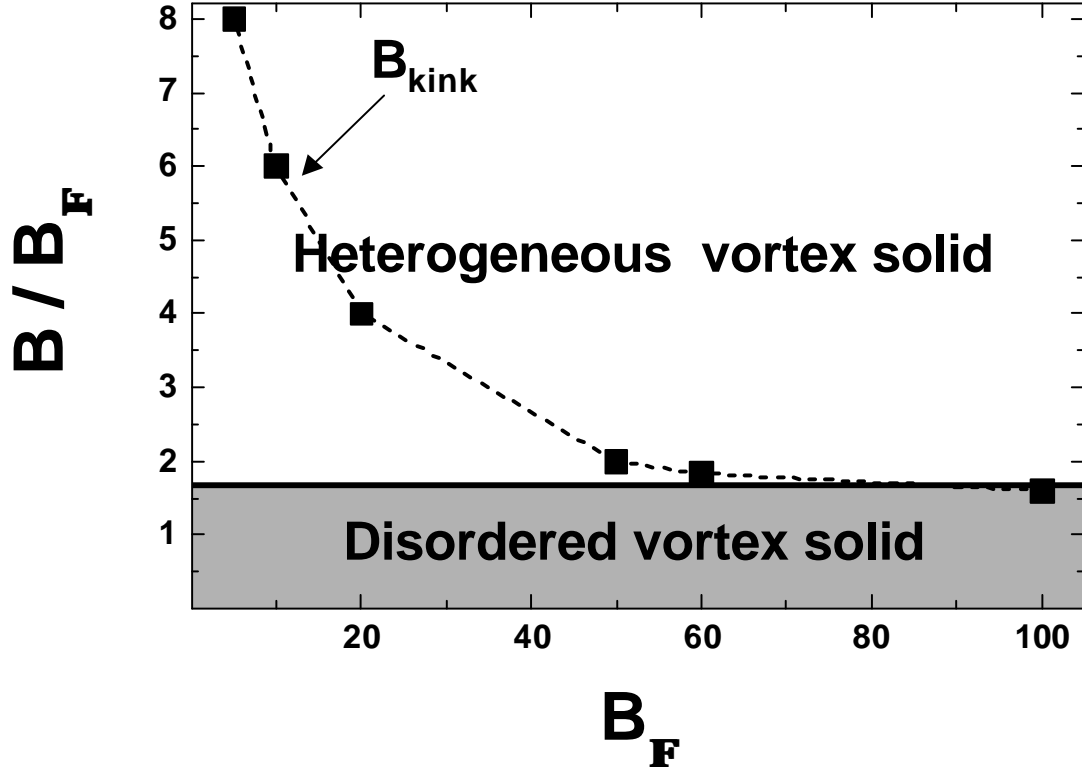


FIG. 12: B_{kink}/B_Φ as a function of B_Φ [19]. The black line at $B/B_\Phi = 1.7$ indicates the boundary between polycrystalline and disordered vortex structures as obtained from the analysis of the experimental ρ_{def} .

ACKNOWLEDGMENTS

M. M. and Y. F. acknowledge financial support from CONICET. M. M. thanks Centro Atómico Bariloche and FOM (Stichting voor Onderzoek der Materie). FC and EZ acknowledge the support by the Fundación Antorchas-WIS collaboration program. Work partially supported by ANPCYT PICT99-5117 by the Israel Science Foundation Center of Excellence and by the US-Israel Binational Science Foundation (BSF).

* *Present address: DPMC, University of Geneva, 24 Quai Ernest-Ansermet, 1211 Geneva 4, Switzerland*

[1] H. Safar, P. L. Gammel, D. A. Huse, D. J. Bishop, J. P. Rice and D. M. Ginsberg, *Phys. Rev. Lett.* **69**, 824 (1992).

- [2] H. Pastoriza, M. F. Goffman, A. Arribere and F. de la Cruz, *Phys. Rev. Lett.* **72**, 2951 (1994).
- [3] E. Zeldov *et al.*, *Nature* **375**, 373 (1995).
- [4] A. Schilling, R. A. Fisher, N. E. Phillips, U. Welp, D. Dasgupta, W. K. Kwok and G. W. Crabtree, *Nature* **382**, 791 (1996).
- [5] D. R. Nelson and V. M. Vinokur, *Phys. Rev. B* **48**, 13060 (1993).
- [6] L. Civale, A.D. Marwick, T.K. Worthington, M.A. Kirk, J.R. Thompson, L. Krusin-Elbaum, Y. Sun, J.R. Clem, F. Holtzberg, *Phys. Rev. Lett.* **67**, 648 (1991).
- [7] M. Konczykowski, F. Rullier-Albenque, E.R. Yacoby, A. Shaulov, Y. Yeshurun and P. Lejay, *Phys. Rev. B* **44**, 7167 (1991).
- [8] S. A. Grigera, E. Morré, E. Osquiguil, C. Balseiro, G. Nieva, and F. de la Cruz *Phys. Rev. Lett.* **81**, 2348 (1998).
- [9] B. Khaykovich, M. Konczykowski, K. Teitelbaum, E. Zeldov, H. Shtrikman and M. Rappaport, *Phys. Rev. B* **57**, R14088 (1998).
- [10] T. Klein, A. Conde-Gallardo, I. Joumard, J. Marcus, C. J. van der Beek and M. Konczykowski, *Phys. Rev. B.* **61**, R3830 (2000).
- [11] D. Grier, C. A. Murray, C. A. Bolle, P. L. Gammel, D. J. Bishop, D. B. Mitzi, and A. Kapitulnik, *Phys. Rev. Lett.* **66**, 2270 (1991).
- [12] R. Cubbit *et al.*, *Nature* **365**, 407 (1993).
- [13] Yanina Fasano, M. Menghini, F. de la Cruz and G. Nieva, *Phys. Rev. B* **62**, 15183 (2000).
- [14] M. V. Marchevsky Ph.D. Thesis, Kamerlingh Onnes Laboratory, Leiden University, Holland. 1996.
- [15] A. Larkin and Y. Ovchinnikov, *J. Low Temp. Phys.* **34**, 409 (1979).
- [16] T. Giamarchi and P. Le Doussal, *Phys. Rev B* **52**, 1242 (1995) and references therein.
- [17] P. Kim, Z. Yao, C. A. Bolle, and C. M. Lieber, *Phys. Rev. B* **60**, R12589 (1999).
- [18] T. Klein, I. Joumard, S. Blanchard, J. Marcus, R. Cubbit, T. Giamarchi and P. Le Doussal, *Nature* **413**, 404 (2001) and references therein.
- [19] S.S. Banerjee, A. Soibel, Y. Myasoedov, M. Rappaport, E. Zeldov, M. Menghini, Yanina Fasano, F. de la Cruz, C. J. van der Beek, M. Konczykowski and T. Tamegai, *Phys. Rev. Lett.* **90**, 087004 (2003).
- [20] M. Menghini, Yanina Fasano, F. de la Cruz, S.S. Banerjee, A. Soibel, Y. Myasoedov, M. Rappaport, E. Zeldov, C. J. van der Beek, M. Konczykowski and T. Tamegai, *Phys. Rev. Lett.*

- 90**, 147001 (2003).
- [21] C. J. van der Beek, M. Konczykowski, V. M. Vinokur, G. W. Crabtree, T. W. Li, and P. H. Kes, *Phys. Rev. B* **51**, 15492 (1995).
- [22] S. S. Banerjee, S. Goldberg, A. Soibel, Y. Myasoedov, M. Rappaport, F. de la Cruz, K. van der Beek, M. Konczykowski, T. Tamegai, V. Vinokur, and E. Zeldov. (unpublished).
- [23] A. Soibel, E. Zeldov, M. Rappaport, Y. Myasoedov, T. Tamegai, S. Ooi, M. Konczykowski and V. Geshkenbein, *Nature* **406**, 282 (2000).
- [24] Yanina Fasano, J.A. Herbsommer, F. de la Cruz, F. Pardo, P.L. Gammel, E. Bucher, and D.J. Bishop, *Phys. Rev. B* **60**, R15074 (1999).
- [25] C. Wengel and U. C. Täuber, *Phys. Rev. Lett.* **78**, 4845 (1997).
- [26] U. C. Täuber and D. R. Nelson, *Phys. Rev. B* **52**, 16106 (1995).
- [27] L. Radzihovsky, *Phys. Rev. Lett.* **74**, 4923 (1995).
- [28] A. V. Lopatin and V. M. Vinokur, *Phys. Rev. Lett.* **92**, 067008 (2004).
- [29] S. Colson, M. Konczykowski, M. Gaifullin, Y. Matsuda, P. Gierlowski, M. Ling, P. H. Kes and C. J. van der Beek, *Phys. Rev. Lett.* **90**, 137002 (2003).